Surface Science 126 (1983) 236–244
North-Holland Publishing Company

SCANNING TUNNELING MICROSCOPY

G. BINNIG and H. ROHRER

IBM Zurich Research Laboratory, CH-88003 Rüschlikon, Switzerland

Received 30 September 1982

Scanning tunneling microscopy, a novel technique based on vacuum tunneling, yields surface topographies in real space and work function profiles on an atomic sale. Surfaces are shown for Au(110), Si(111) and GaAs(111).

1. Introduction

Tunneling spectroscopy has developed into a field of intensive research since its first application to superconductors by Giaever [1] in 1961. Subsequently, it was extended to surface studies, mainly through inelastic tunneling spectroscopy [21]. In general, tunneling experiments are performed with metal–insulator–metal (or semiconductor) sandwich structures with a solid-state insulator. This classical tunneling technique evidently has two inherent limitations: (1) once the tunnel junction has been made, access to the electrode surfaces for further treatment and investigations is lost, and (2) the information is averaged over an area limited in smallness by current lithographic techniques, i.e., > 1000 Å. However, using vacuum as tunnel barrier provides both access to the tunnel electrodes at any time and, by appropriately shaping one of the electrodes, a spatial resolution far beyond that of sandwich structures. In addition, vacuum is conceptually the most simple tunnel barrier, and experiments pertain directly to the properties of the electrodes and their bare surfaces. Vacuum tunneling offers fascinating and challenging possibilities in surface physics and many other areas, left to the reader's imagination. This paper deals mainly with the easiest application of vacuum tunneling, the *Scanning Tunneling Microscope (STM)*, which yields surface topographies on an atomic scale directly in real space. Our interest in scanning tunneling microscopy up to now has focussed mainly on exploring its potential (metals, semiconductors, decoration techniques) and demonstrating its unprecedented resolution [3,4]. For comprehensive surface studies, vacuum tunneling has to be performed together with other surface techniques. Such efforts are in progress.

0039-6028/83/0000–0000/$03.00

2. Principle of the scanning tunneling microscope (STM)

The principle of the STM is straightforward. It consists essentially in scanning a metal tip (one electrode of the tunnel junction) over the surface to be investigated (second electrode), as depicted in fig. 1. (Note that distances and sizes are not to scale.) The metal tip is fixed to a rectangular piezodrive P_x, P_y, P_z, made out of commercial piezoceramic material. The tunnel current J_T is a sensitive function of the gap width s, i.e., $J_T \propto V_T \exp(-A\phi^{1/2}s)$, where ϕ is the average barrier height (work function) and $A \approx 1$ if ϕ is measured in eV and s in Å. With work functions of some eV, J_T changes by an order of magnitude for every ångström change of s. The control unit CU applies a voltage V_z to the piezo P_z such that J_T remains constant when scanning the tip with P_y and P_x over the surface. At constant work function ϕ, $V_z(V_x, V_y)$ yields the topography of the surface, $z(x, y)$, directly, as illustrated at a surface step at A. Smearing of the step, δ, is of the order $\sqrt{R(\text{Å})}$, where R is the radius of curvature of the tip [4]. For constant tunnel current, changes in the work function are compensated by corresponding changes in s. Thus, a lower work function at a contamination spot C would mimick the surface structure B. Work-function-induced structures and true structures can, however, be separated by modulating the tunnel distance s by Δs while scanning, at a frequency higher than the cutoff frequency of the control unit (at a lower frequency, the modulation would simply be compensated by the feedback loop). The modulation signal $J_s = \Delta(\ln J_T)/\Delta s \approx \phi^{1/2}$ directly gives the work function in a simple situation as shown in fig. 1. In general, however, $\Delta s = \Delta z \cos \varphi$, where Δz is the length modulation of the piezo P_z and φ the angle between the z direction and grad(z). Separation is then, although involved, still

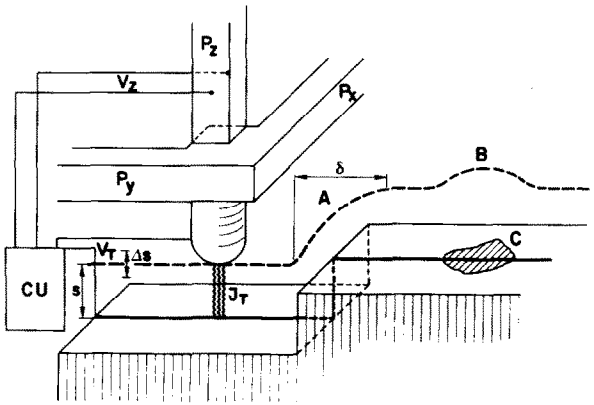

Fig. 1. Principle of the operation of the Scanning Tunneling Microscope (STM). © 1982 The American Physical Society.

possible, since V_z and J_s contain topography and work function in a different way.

3. Apparatus

Some crucial parts of the tunnel unit are sketched in fig. 2. Stability of a vacuum gap in the sub-Å range and a lateral resolution in the Å range requires excellent vibration damping and very sharp tunnel tips.

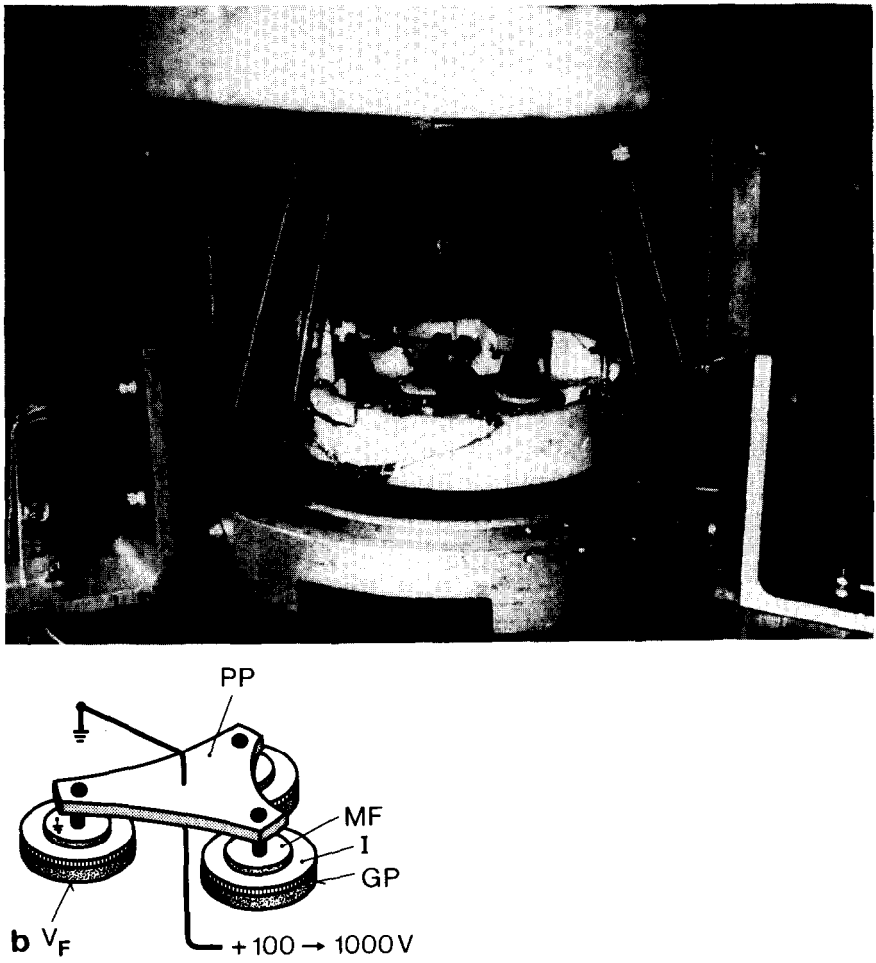

Fig. 2. (a) Tunnel unit showing piezodrives with tunnel tip (left) and sample mounted on "louse" (right). (b) Schematic of the "louse".

(a) *Vibration damping* was initially achieved with superconducting magnetic levitation. At present, we use a two-stage spring system, and a stability of the gap width of about 0.2 Å is reached. Fig. 2a shows the tunnel unit with the rectangular piezodrives to which the tunnel tip is attached and the rough motion system with the sample holder and heater. The piezodrives cover only some micrometers in each direction. It is important that sample and tip can be approached vibration-free to within working range of the piezodrives to avoid accidental contact of tip and sample. The rough drive also serves for separation in cleaning procedures of the sample ($\approx$ 1 cm) and to compensate for thermal expansions when working at elevated temperatures (up to 100 μm). The rough drive, named the "louse", is sketched in fig. 2b. Its body consists of a piezoplate (PP), with sample holder on top (not shown) and resting on three metal feet (MF), separated by high dielectric-constant insulators (I) from the metal groundplates (GP). The feet are clamped electrostatically to the groundplate by applying a voltage V_F. Elongating and contracting the body of the louse with the appropriate clamping sequence of the feet moves the louse in any direction in steps between 100 Å to 1 μm and up to 30 steps/s.

(b) *Tunnel tips*. A key factor for the lateral resolution of the STM is the radius of curvature of the tip. Field-emission tips have radii of the order of 100 Å. However, they are long and narrow and therefore vibration-sensitive. In addition, occasional contact of tip and sample cannot yet be avoided. The tips used at present are made of W or Mo wires of about 1 mm diameter, ground at one end at roughly 90°. This yields tips of overall radii of < 1 μm, but the rough grinding process creates many rather sharp minitips. The extreme sensitivity of the tunnel current on gap width then selects the minitip closest to the sample for tunneling. This yields a lateral resolution of about 20 Å. In-situ sharpening of the tip by gently touching the surface brings the resolution down to the 10 Å range; by applying high fields (order of 10^8 V/cm) during, say, half an hour, resolutions considerably below 10 Å could be reached.

The piezodrive materials were calibrated with a capacitance dilatometer, giving an overall accuracy of better than 5%. Finally, it should be mentioned that the tunnel unit in use required no precision machining. Problems mainly arise from the required UHV compatibility of all the parts used. UHV is needed to control surface conditions, but is not required to perform vacuum tunneling.

4. Surface topography

Scanning tunneling microscopy with a depth resolution in the sub-Å range and a lateral resolution of a few Å provides an attractive, unique approach to surface topography on an atomic scale. One expects a deeper and detailed understanding of regular surface structures, i.e., surface reconstructions, and

new information on irregular surface structures like surface roughness, formation of steps and growth phenomena. In the following, we present some results on both regular and irregular surface structures.

(a) *Au(110) surface.* The reconstruction of the Au(110) surface, although extensively studied experimentally and theoretically [5], is not well understood. A variety of reconstructions is found, ranging from very large periodicities to a hexagonal topmost layer. Of particular interest is the 1×2 reconstruction, which none of the proposed models explains comfortingly. Fig. 3 shows a STM picture of an Au(110) surface under UHV conditions (5×10^{-10} Torr) at (a) room temperature and (b) 300°C, after the standard surface treatment to obtain reconstructions (clean sputtering and subsequent annealing at 600°C in UHV). At room temperature, the surface was usually smooth but gently buckled with a wavelength between 30 and 50 Å, and amplitudes between half an Å to 2 Å. Surface steps were scarce and the four-layer step across the upper-left corner in the [1$\bar{1}$0] direction is an exception. At 300°C, steps were abundant. It is tempting to relate this surface roughening to the disappearance of surface reconstructions above around 400°C. From the observed sharpness of the steps, it was conjectured that the 2×1 reconstruction, if at all present, should be of the smooth type (e.g., distorted topmost hexagonal layer model), with the wavy structure responsible for the directed diffusivity of the LEED peaks. In the meantime, we found that exposure to high electric fields can

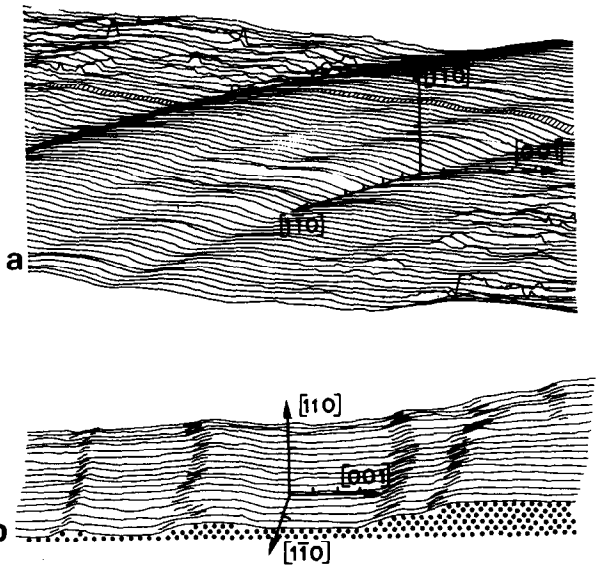

Fig. 3. Topography of an Au(110) surface on a scale of 10 Å per division at (a) room temperature, (b) 300°C, possible Au positions indicated by the dots. © 1982 The American Physical Society.

sharpen the tip, so that the experimental resolution of figs. 3a and 3b is not necessarily the same. Indeed, the most recent experiments show ribbons of clearly resolved 1×2 reconstructions, separated by 1×3 and less frequently 1×4 structures. The 1×2 reconstruction extends over hundreds of Å in the $[1\bar{1}0]$ direction, but only a few periods in the [001] direction, considerably smaller than the coherence length in scattering experiments. Its corrugation appears symmetric and considerably stronger than expected from the pairing-row model. The strong and symmetric corrugation of the 1×3 reconstruction indicates that two top-layer rows and one second-layer row are missing, giving rise to two (111) facets. This tendency to form (111) facets favors the missing-row model for the 1×2 reconstruction. A detailed account of the Au(110) surface will be given elsewhere.

(b) *The Si(111) surface.* The 7×7 reconstruction of the Si(111) surface is another intriguing problem. A recent proposal is a weakly corrugated, partially or fully developed 7×7 structure (compatible with LEED experiments) on a terraced surface with steps of 3.05 Å and terrace size of several 7×7 unit cells (to account for the oscillatory behavior of the specular beam in He-diffraction experiments [6]). Initial STM experiments on a crystal known to produce a 7×7 structure exhibited an array of equilateral triangles with strong corrugation only at the corners. Towards the middle of the triangles, the corrugation became very weak (< 0.5 Å). However, due to calibration problems of the tunnel unit used, we were not able to determine the triangle size. Subsequent experiments on other Si crystals (the initial one got destroyed in an annealing procedure) could not yet reproduce the 7×7 structure. We believe this to be

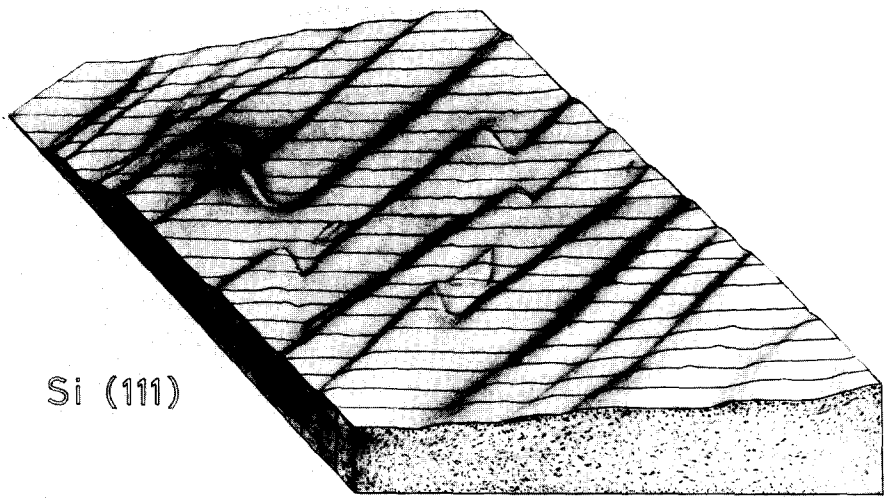

Fig. 4. Topography of a Si(111) surface, with monoatomic step lines of 3 Å height.

due to carbon which diffused to the surface in the annealing process, as seen by subsequent Auger analysis. Instead, a great number of [$\bar{2}11$] steps of 3 Å height and up to 50 Å apart were found, as shown in fig. 4. The lateral step resolution is usually better than 10 Å. The steps are connected through angles of 60°. This is to be expected if the steps are all of the same type, a reasonable assumption. ($\bar{2}11$) steps have only one broken bond, whereas ($2\bar{1}\bar{1}$) steps have two, and therefore the ($\bar{2}11$) steps should be a better choice. However, cleaved Si(111) surfaces exhibit only $2\bar{1}\bar{1}$ steps extending over many μm. Pandey [7] has proposed a step relaxation where the edge hexagon relaxes to a pentagon, which takes care of the extra broken bonds. At first sight, it seems reasonable that annealing favors even more such low-energy pentagon steps. On the other hand, cleaving does not produce the 7×7 reconstruction either. Therefore, it appears that annealing and cleaving not only lead to different reconstructions, but also to different types of steps. Alternatively, the same mechanism, which suppressed the 7×7 structure in our crystals, might favor ($\bar{2}11$) steps. This is an interesting problem in itself. Although the 7×7 problem has not yet been solved, the present results are encouraging, and scanning tunneling microscopy hopefully will contribute to a better understanding of this problem.

(c) *GaAs(111) facets.* Nomarsky micrographs indicate that liquid-phase epitaxy produces flat GaAs(111) facets (roughness smaller than 10 Å) with very few growth centers and rather regular steps of the order of 10 Å and 6 μm apart [8]. Scanning tunneling microscopy verified that the facets are indeed atomically flat over regions of some hundred Å linear dimensions [9]. Such a micrograph, including a double step, is shown in fig. 5. Fig. 5a illustrates a surface step at an angle α with respect to the scanning direction, indicated by the four lines across the surface. The actual scans of fig. 5b coincide on the flat

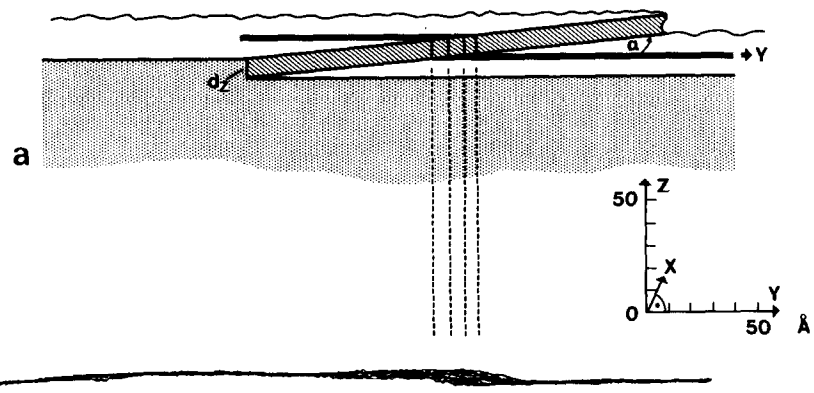

Fig. 5. GaAs(111) facets. (a) Schematic of step at angle α with scanning direction (Y). (b) STM picture viewed in the x-direction. After ref. [9].

parts of the surface and give a side view of the step. The crystals were grown some years ago and blue reflectance indicated surface oxide of several 100 Å which was dissolved by HCl. After etching, Nomarski microphotographs showed the same surface features as previously, indicating that oxidizing and subsequent etching do not roughen the facets appreciably. No further surface cleaning was applied in order to keep the growth surface as intact as possible. STM investigations of semiconductors require high electric fields (some volts over a gap of some 10 Å for quenching the Schottky layer) which lead to field-induced desorption of adsorbates and thus noisy signals. For noise reduction, a 100 to 200 Å Au film was sputter deposited, preserving the surface features seen by Nomarski. The STM picture of fig. 6 was taken on a gold-coated surface, but the uncoated GaAs gave similar results except for considerbly larger noise. The scans nearly overlap on the flat areas, whereas at the step, which makes an angle α with the Y-direction, the contour lines are better separated. The measured step height of 6 to 7 Å corresponds to a double layer of $2 \times d_{(111)} = 6.5$ Å. On both sides of the step, the surface is flat within less than 2 Å, thus atomically flat. It is interesting to note that oxidizing to several hundred Å appears to be homogeneous on an atomic scale. The most interesting aspect for the scanning tunneling microscopy, however, is that both etching and the gold coverage retain the sharpness of the step to a great extent so that it appears only 20 Å wide. Metal decoration is a well-accepted technique in phase-contrast microscopy, and is known to preserve gross surface features. That it also retains steps on a nearly atomic scale is unexpected and also important, since it provides possible extension of the STM technique to insulator surface studies.

(d) *Au islands on Si.* The last example illustrates the use of scanning tunneling microscopy for work-function studies. This technique has not yet been developed in detail, and was used in the foregoing examples only to

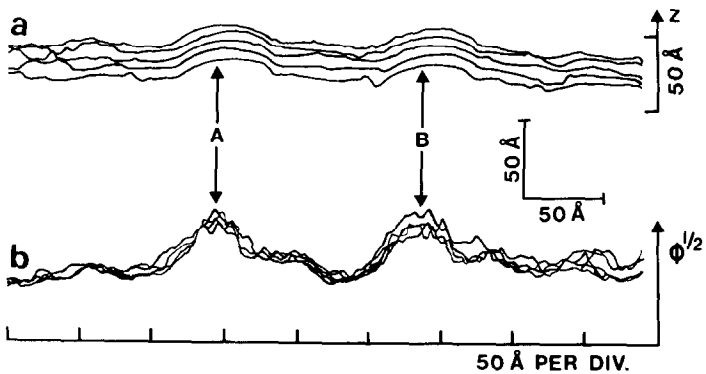

Fig. 6. Au islands on Si: (a) STM topography; (b) corresponding work-function scans.

obtain a general impression of the surface conditions. Thus, the present example should rather be taken as an exploratory effort on this technique. A slight coverage of Au on a Si surface is expected to produce Au islands. Fig. 6a is a topographic picture. It shows predominantly a rough surface with two smooth hills at A and B. It seems reasonable to associate the rough parts with the Si surface (untreated and certainly somewhat oxide-covered) and the smooth hills with Au islands. In the work-function profile of fig. 6b, the two Au islands are clearly resolved, although the noise is still appreciable. Since the zero of the measured work function is not known, no direct contact can be made with the actual work functions of Si and Au. Nevertheless, this example leads to the expectation that work-function profiles should eventually be resolved with a resolution similar to that in topographies.

In summary, these initial results demonstrate that scanning tunneling microscopy shows a great potential for surface studies. Even more, the possibility of determining work functions and performing tunneling spectroscopy with atomic resolutions should make vacuum tunneling a powerful technique for solid-state physics and other areas. Of course, there still remain many technological (e.g., ultimate control of the sharpness of the tunnel tip) and scientific (e.g., tunneling in small, non-planar geometry) problems to be solved, in order to fully exploit the potential of vacuum tunneling.

Acknowledgements

We should like to thank Hans-Ruedi Ott for calibrating the piezodrives, Karl-Heinz Rieder for discussions on surface aspects, and Christoph Gerber and Edmund Weibel for valuable technical assistance.

References

[1] I. Giaever, Phys. Rev. Letters 5 (1961) 147.
[2] For references, see T. Wolfram, in: Inelastic Electron Tunneling Spectroscopy, Springer Series in Solid State Sciences, Vol. 4 (Springer, Heidelberg, 1978).
[3] G. Binnig, H. Rohrer, Ch. Gerber and E. Weibel, J. Appl. Phys. 40 (1982) 178.
[4] G. Binnig, H. Rohrer, Ch. Gerber and E. Weibel, Phys. Rev. Letters 49 (1982) 57.
[5] See H.P. Bonzel and S. Ferrer, Surface Sci. 118 (1982) L263.
[6] N. Garcia and J.M. Soler, 2nd General Conf. of the Condensed Matter Division of the EPS, Manchester, 1982.
[7] K.C. Pandey, Phys. Rev. Letters 47 (1981) 1913;
K.C. Pandey, to be published.
[8] H.J. Scheel, Appl. Phys. Letters 37 (1980) 70.
[9] H.J. Scheel, G. Binnig and H. Rohrer, J. Crystal Growth 60 (1982) 199.